Simulation Standard

Connecting TCAD To Tapeout

A Journal for Process and Device Engineers

Simulation and Characterization of High-Frequency Performances of Advanced MIM Capacitors

J.Piquet(1), O.Cueto(2), F.Charlet(3), M.Thomas(4), C.Bermond(1), A.Farcy(4), J. Torres(4), B.Fléchet(1)

(1) LAHC, Université de Savoie, Bâtiment Le Chablais, 73376 Le Bourget du lac cedex, France.
(2) CEA/DRT-LETI/D2NT-CEA/GRE, 17 rue des Martyrs, 38054 Grenoble Cedex 9, France.
(3) SILVACO. 55 rue Blaise Pascal 38330 Montbonnot St Martin France.
(4) STMicroelectronics, 850 rue Jean Monnet, 38926 Crolles cedex, France
jerome.piquet@etu.univ-savoie.fr, olga.cueto@cea.fr,
francois.charlet@silvaco.com, maryline.thomas@st.com

Abstract:

High-frequency simulations and characterizations of advanced metal-insulator-metal (MIM) capacitors with ultra thin 32 nm PECVD Si_3N_4 dielectric are presented. The frequency dependent behavior of capacitors is numerically and experimentally extracted over a wide frequency bandwidth. Numerical results are validated by comparison to experimental results. An equivalent circuit model of capacitors including four parameters is developed for a better understanding of the frequency dependent behavior. We focused on the impact of design on the performances of MIM capacitors realized on Si substrates.

1. Introduction

The Metal-Insulator-Metal capacitor is a key passive component in Radio Frequency (RF) and analog integrated circuits. MIM capacitors have attracted great attention because of their high capacitance density that supplies small area, increases circuit density, and further reduces the fabrication cost. They provide good voltage linearity properties. Developments focus on capacitance density increase through the introduction of high-k materials to replace Si_3N_4 (k ~ 7) and 3D high-density architectures.

The improvement of performances thanks to Cu introduction in interconnects naturally leads to the integration of copper as a metal electrode for MIM capacitors. The objective is to improve the quality factor by reducing parasitic resistances and ensure the compatibility of MIM capacitor integration scheme with copper interconnect one. The required damascene architecture was first presented for TiN/Si_3N_4/TiN MIM capacitors [1]. Here, a Cu/Si_3N_4/TaN/Cu stack is implemented between M5 (metal5) and M6 (metal6) levels. Such MIM capacitors have been integrated among multilevel copper interconnects in a 120 nm technology node, using Si_3N_4 to reach 2 fF/μm^2 capacitances.

Special attention is paid on high-frequency performances as RF and analog applications are targeted. A new 3D electromagnetic simulator (***QUEST***) is used to predict electrical performances of MIM capacitors. High frequency characterizations coupled with ***QUEST*** results are carried out to evaluate the impact of both the introduction of copper and the design of electrodes on performances.

2. Simulation and Characterization

The goal of this paper is to present a complete methodology to analyze and predict MIM capacitors performances built on a reliable and efficient 3D simulation tool validated by comparison with measurements. An electrical model of MIM capacitors is extracted from scattering parameters to obtain a better understanding of the frequency behavior of the capacitors.

Continued on page 2 ...

INSIDE

Numerical Analysis of GaInP Solar Cells: Toward Advanced Photovoltaic Devices Modeling 6
Calendar of Events 10
Hints, Tips, and Solutions 11

SILVACO INTERNATIONAL

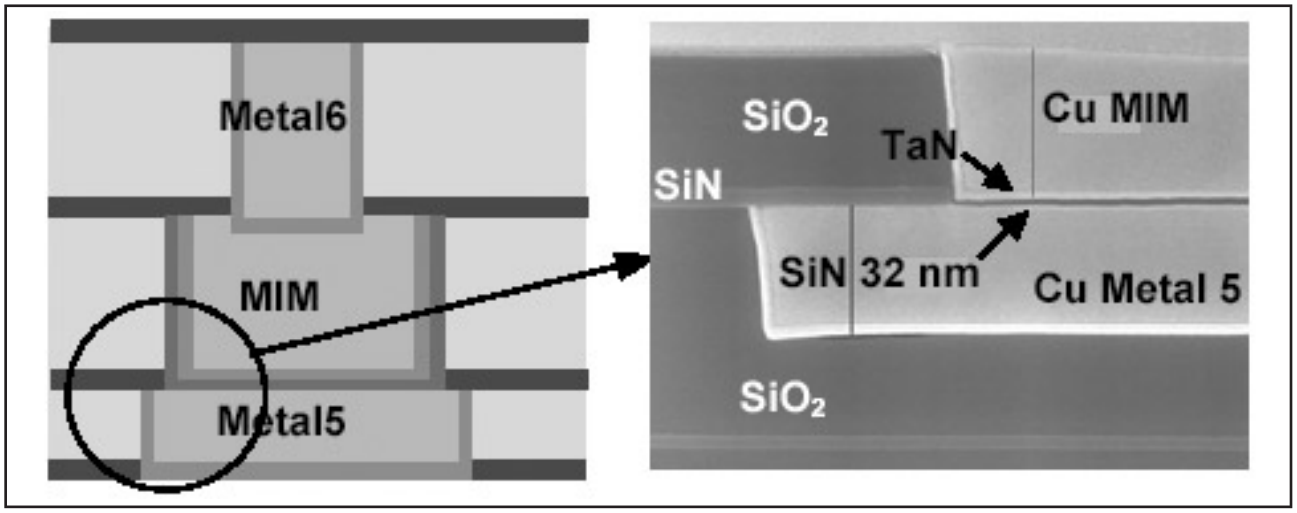

Figure 1. Schematic and MEB cross-sections of the damascene MIM capacitor stack integrated between M5 and M6 levels.

2.1 Test Structure Description

Dedicated MIM capacitor test structures were fabricated on 200 mm silicon substrates with a resistivity of 5.5 S/m. After completion of M5 level, the MIM cavity is etched in the V5 inter-level dielectric (SiO2) down to a M5 copper interconnect, which is used as a bottom electrode. Next, a 32 nm thick Si_3N_4 film is deposited by PECVD (Plasma Enhanced Chemical Vapor Deposition) in the cavity, before metallization with deposition of a TaN/Ta barrier, which acts as a top electrode, and Cu filling. Materials in excess are then removed by CMP (Chemical and Mechanical Polishing). Finally, V5 and M6 levels are completed. The resulting $Cu/Si_3N_4/TaN/Cu$ stack is connected through M5 and M6 levels, as shown in Figure 1.

The design of such damascene capacitors has to meet copper density requirements. Thus, specific designs with comb or grid electrodes were introduced. Figure 2 illustrates the structures particularly studied. Two structures have been selected for this study. C_1 and C_2 are different designs of grid electrodes with the same area (3 300 μm^2) leading to a capacitance of 6.6 pF. Each elementary single line of the grid is 12 μm wide.

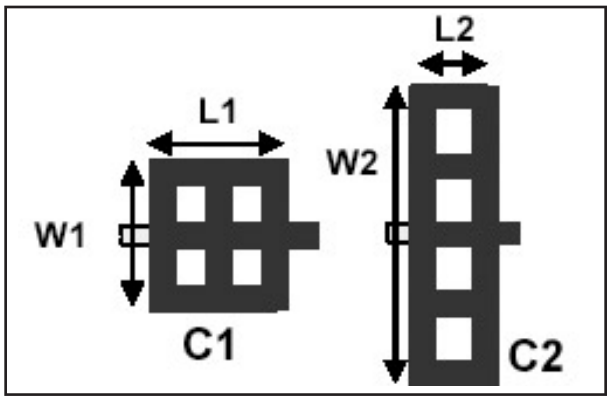

Figure 2. Top views of studied MIM capacitors. W1 = 66 µm, L1 = 66 µm, W2 = 120 µm, L2 = 39 µm.

All MIM capacitors are integrated between M5 and M6 levels. As M6 is a thick level ensuring the lowest resistance, access lines are dissymmetric in spite of an identical width of 10 μm (Figure 3). These dissymmetrical Metal5 and Metal6 access lines are connected to RF pads.

High-frequency behavior of such MIM capacitors is poorly known. So, DC and RF electrical characterizations are carried out to evaluate capacitor performances. A general equivalent electrical model is defined and checked over a large range of frequency (typically from 40 MHz to 25 GHz). Moreover, the impact of MIM capacitor design on its performances is investigated.

Capacitor access lines are connected to RF pads in order to contact measurement probes. Capacitance is measured using a HP4274A multi-frequency LCR meter at frequencies ranging from 100 Hz to 100 KHz. Scattering parameters are extracted using an ANRITSU 37397C Vector Network Analyzer after a TRL (Thru Reflect Line) calibration de-embedding technique [2]. This technique enables to eliminate discontinuities fromcontact pads to access lines and places the reference planes at both ends of capacitors (P1-P2). Thus, only MIM capacitor characteristics are measured.

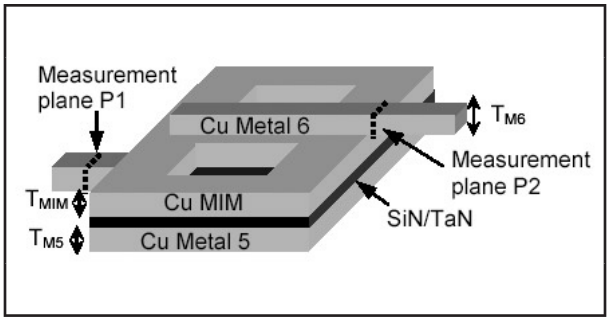

Figure 3: 3D view of MIM capacitor, where TM6 ~ 800 nm, TM5 ~ 300 nm, and TMIM ~ 400 nm.

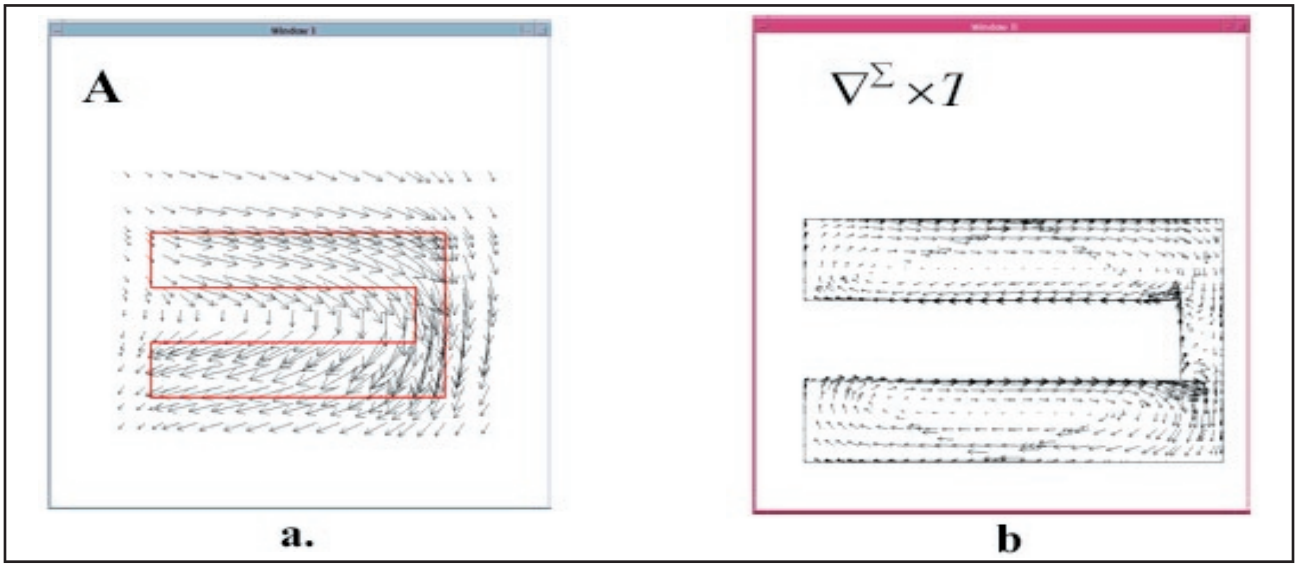

Figure 4. a) Magnetic Potential vector (A) and b) Density of Current ($\nabla_{\Sigma} x\, T_e^{\Sigma}$)

2.2 3D Electromagnetic Simulation

2.2.1 Presentation of the new simulation tool

The simulations are carried out using the 3D electromagnetic field solver called ***QUEST***. This simulator calculates the electromagnetic parameters of micro-electronic 3D geometries in frequency domain. It can extract Z, Y, S matrices and quality factors of Nports general structures.

QUEST is based on a 3D field solver elaborated by SILVACO in collaboration with CEA-LETI [3][4]. It uses an original formulation of the Quasi-Static Maxwell equations where the problem is separated in two parts, an impedance and a capacitance part.

The impedance problem is written using a (A, T^{Σ}) formulation [5], where A is the magnetic potential vector, T^{Σ} is an equivalent vector electric potential defined on the conductors surface, μ is the permeability and σ^{Σ} is a surfacic conductivity that approximates the volumic conductivity and takes into account the skin effect. With this formulation, A and T^{Σ} are solution of :

$$\nabla x\, \mu_{-1}\, \nabla x\, A - \nabla_{\Sigma} x\, T^{\Sigma} = 0$$

$$\nabla_{\Sigma} x (\sigma\Sigma)^{-1} \nabla_{\Sigma} x\, T^{\Sigma} + j\omega \nabla x A = 0$$

The magnetic potential vector A is calculated using edge finite elements [6] on a 3D regular grid (Figure 4). The electric potential vector T^{Σ} is calculated using scalar P1 elements on a triangle meshing of the conductors surfaces (Figure 2b).

The capacitance problem comes from the equation:

$$\nabla_{\Sigma} (z\Sigma)^{-1}\ \nabla_{\Sigma\phi\Sigma} = j\omega p\Sigma$$

where ϕ^{Σ}, p^{Σ} are the surface potential and the surface electric charge. z^{Σ} is a local impedance given by the impedance problem. The capacitance problem is solved using a fast and accurate computation method so called « fictitious domain method » [3].

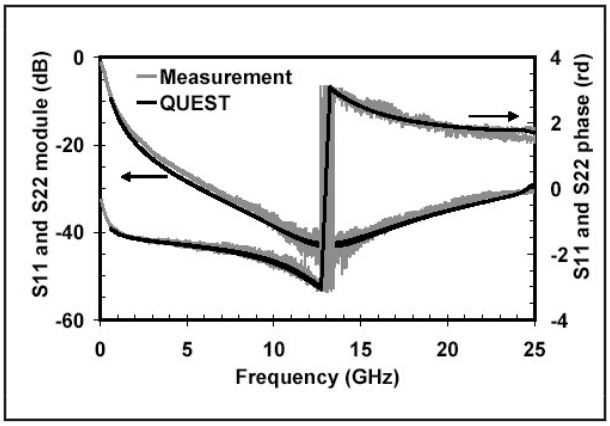

Figure 5. Module and phase of reflexion parameters resulting from both measurement and QUEST simulator for C1 structure.

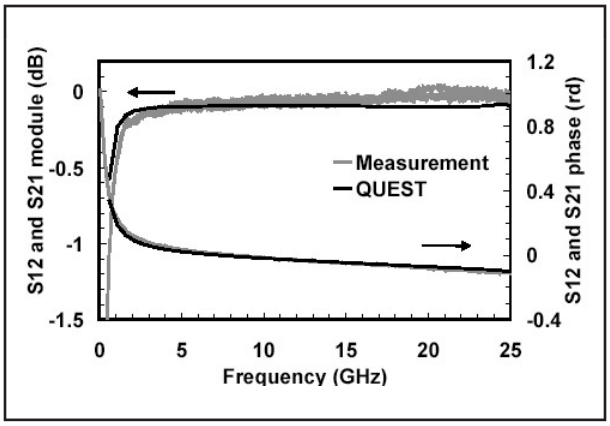

Figure 6. Module and phase of transmission parameters resulting from both measurement and QUEST simulator for C1 structure.

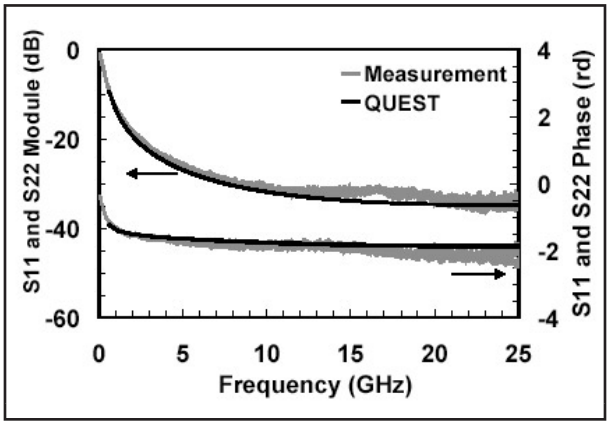

Figure 7. Module and phase of reflexion parameters resulting from both measurement and QUEST simulator for C_2 structure.

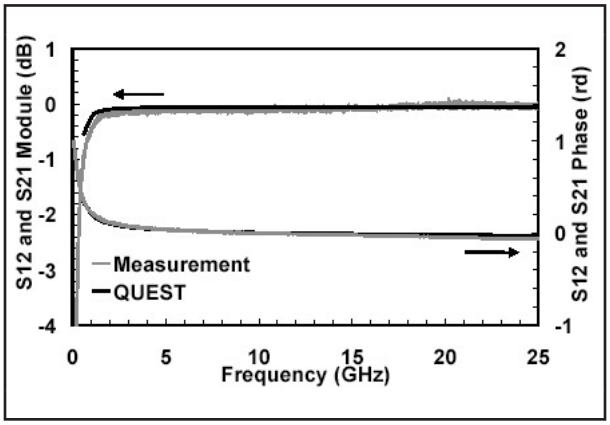

Figure 8. Module and phase of transmission parameters resulting from both measurement and ***QUEST*** simulator for C_2 structure.

2.2.2 Validation of the numerical results

To validate the electromagnetic simulations, a comparison with measurements is presented. Two structures C_1 and C_2 were simulated with ***QUEST***. Associated 3D dimensional structures were created from GDS and technology files using the ***QUEST*** Graphical User Interface. The simulations were performed on a Sun fire V440 station with 4 ultra Sparc III1 CPUs and the corresponding CPU times calculations with 80 frequency points from 100 MHz to 25 GHz are about three hours. Results are presented in Figures 5 to 8.

An excellent similitude between measurement and ***QUEST*** results is observed for C1 and C2 structures. Module and phase evolution resulting from measurement and ***QUEST*** simulation have nearly the same behavior. Thus, ***QUEST*** is an efficient and accurate tool to evaluate the high frequency behavior of MIM capacitors.

To improve the study, impact of design on MIM capacitors electrical performances is then evaluated.

2.3 Impact of Design on Capacitors Performances

To investigate the MIM capacitor characteristics at RF regimes, scattering parameters and characteristic impedance of access lines have first to be extracted. M5 level access lines are thinner than M6 ones, leading to different propagation constant on the two access ports. A dissymmetrical calibration de-embedding technique is performed. However, the characteristic impedance of each level access line is calculated and their values are identical. Then, for the following extraction, M5 and M6 access lines are considered to have the same complex characteristic impedance Z_0. The complex impedance of MIM capacitor is also extracted.

As the longest MIM capacitor is 66 μm (in the direction of propagation), and the maximum frequency measurement is 25 GHz, corresponding to a wavelength of 4.5 mm, MIM capacitors are considered as localized elements (i.e. no propagation effect occurs among electrodes) characterized by the serial complex impedance Z_S. Scattering parameters and Z_0 impedance of measurement references planes (P1 and P2) are used to calculate the B element of the transfer matrix ABCD. Then, Z_S MIM capacitor impedance is directly extracted as following equation shows:

$$Z_s = Z_0 \frac{(1+S_{11})(1+S_{22}) - S_{12}S_{21}}{2S_{21}}$$

As a next step, MIM capacitors impedance Z_S is extracted from both measurements and ***QUEST***.

2.3.1 Modeling

For a better understanding of MIM capacitor behavior in a high-frequency regime, an equivalent circuit model is established as shown in Figure 9 and discussed. The elements C and Rp figure the basic model for the capacitor, whereas additional series Rs and Ls represent the parasitic resistance and inductance due to the specific electrode design [7]-[11]. Notice that the shunt Rp is originated from dielectric losses that brings on power dissipation.

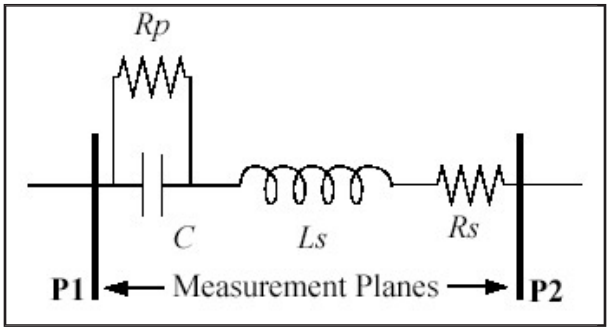

Figure 9. Equivalent electrical model of MIM capacitors extracted at a high-frequency regime. Measurement plane references are at the capacitor borders.

Thus, impedance of this model was calculated and its real and imaginary parts were clearly identified. Coupled with the Z_S MIM capacitor impedance, each element of the equivalent circuit model is extracted using the entire frequency range.

This method is used to determine each of the four parameters, C, Rp, Rs and Ls, that appears in the equivalent circuit model and their values can be seen in Table 1.

The capacitance values of the two structures were verified by performing measurement with a LCR meter, resulting in a 6.65 pF capacitance for C_1 and C_2. Both accuracy and repeatability of this extraction were demonstrated thanks to a gap capacitance value less than 3 % between same area structures. It was also proved that static results and extracted high-frequency results are similar.

Design of MIM capacitors doesn't act upon resistive elements Rs and Rp. However, for the same area structures, so with an identical capacitance value, when the capacitor length (L) is divided by a factor two, the inductive element Ls is divided by the same factor.

This result shows the relationship between length capacitor and parasitic inductance (Ls). Extraction results confirm that the best MIM capacitor grid design is C2 for an area of 3300 μm^2. So, as a design recommendation, the length of electrodes has to be minimized.

Extracted elements from measurements are very closed to extracted ones from ***QUEST***. Error percentage is less than 3% on C element and 10% on Ls element.

This method represents a very good solution to evaluate the electrical performances of MIM capacitors. Coupled with the new 3D electromagnetic simulator, efficient and competitive design having best high frequency behavior, could be integrated among new generation of damascene MIM capacitors.

3. Conclusions

From previous results, high-frequency behavior of damascene MIM capacitors integrating copper electrodes is simulated to investigate electrical performances as a function of design and material parameters. Accuracy and efficiency of a new 3D electromagnetic simulator called ***QUEST*** is established. With this simulator, impact of new high-k dielectrics and new designs on MIM capacitor electrical performances can be predicted for future generations of RF integrated circuits based on these results. New materials, like Ta_2O_5, will increase the capacitance value and new design will be required to reduce the parasitic serial inductance in order to enable high-performance MIM capacitor integration for high frequency applications.

	Structures	Element values			
		Rs (Ω)	Rp (KΩ)	C (pF)	Ls (pH)
Measurement	C1	0.20	0.36	6.59	45.5
	C2	0.15	0.39	6.75	22.0
QUEST	C1	0.25	0.60	6.79	42.2
	C2	0.19	0.65	6.92	19.9

Table 1. Element values of equivalent circuit model.

References:

[1] A. Farcy, J. Torres, V. Arnal, M. Fayolle, H. Feldis, F. Jourdan, M. Assous, J.L. Di Maria, V. Vidal, "A new Damascene Architecture for High-Performances Metal-Insulator-Metal capacitors Integration", Materials for Advanced Metallization conference, pp 368-372, La Londe Les Maures, 2003.

[2] B. Fléchet, K, Kouicem, A, Benhayoun, G, Angénieux, "Développements relatifs aux procedures d'auto calibrage TRL ; correction d'erreurs systématiques résiduelles et calibrage dissymétrique", 9eme Journées Nationales Microondes, JNM 1995, 4-6 avril 1995, Paris, France.

[3] S. Putot, F. Charlet, P. Witomski, "A fast and accurate computation of interconnect capacitances" International Electron Devices Meeting, pp 893-897, Washington, 1999.

[4] F. Charlet, J.F. Carpentier, "Extraction of 3D interconnect impedances using edge elements without gauge condition" Simulation of Semiconductor Processes and Devices conference, 2002.

[5] D. Albertz, G. Henneberger, "On the use of the new edge based A-A,eT formulation for the calculation of time harmonic stationary and transient eddy current field problems" . IEEE Transactions on Magnetics. Vol 36, no 4, july 2000, pp 818-822.

[6] J.C. Nedelec. "Mixed finite elements in R3", Numerische mathematic.(1980), 35, pp315-341.

[7] S. B. Chen, C. H. Lai, Albert Chin, J. C. Hsieh and J. Liu, "RF MIM capacitors using High-K Al2O3 and AlTiOx dielectrics" IEEE Microwave Symposium Digest, Vol. 1, pp. 201-204, 2002.

[8] X. F. Yu, Chunxiang Zhu, H Hu, Albert Chin, MF Li, BJ Cho, D.-L. Kwong, MB Yu, and PD Foo, "A high density MIM capacitors (13fF/um2) using ALD HfO2 dielectrics" IEEE Electron Device Letters, Vol. 24, No. 2, pp. 63-65, 2003.

[9] Chen, S.B.; Lai, C.H.; Chan, K.T.; Chin, A.; Hsieh, J.C.; Liu, J. "Frequency-dependent capacitance reduction in high-k AlTiOx and Al2O3 gate dielectrics from IF to RF frequency range " IEEE Electron Device Letters, Vol. 23, Issue 4, pp. 203-205, 2002.

[10] Jae-Hak Lee; Dae-Hyun Kim; Yong-Soon Park; Myoung-Kyu Sohn; Kwang-Seok Seo, "DC and RF characteristics of advanced MIM capacitors for MMIC's using ultra-thin remote PECVD Si3N4 dielectric layers" IEEE Microwave and Guided Wave Letters, Vol. 9, Issue 9, pp. 345-347, 1999.

[11] M.Y. Yang, C.H. Huang, A. Chin, C. Zhu, M.F. Li, and D.-L. Kwong, "High density MIM capacitors using AlTaOx dielectrics," IEEE Electron Device Letters, Vol. 24, No. 5, pp. 306-308, 2003.